Astronomy
&
Astrophysics

Removing $1/f$ noise stripes in cosmic microwave background anisotropy observations

D. Maino[1], C. Burigana[2], K. M. Górski[3,4], N. Mandolesi[2], and M. Bersanelli[5]

[1] Osservatorio Astronomico di Trieste, via G.B. Tiepolo 11, 34131, Trieste, Italy
[2] Istituto TeSRE, Consiglio Nazionale delle Ricerche, via Gobetti 101, 40129, Bologna, Italy
[3] ESO, European Southern Observatory, Karl-Schwarzschild Str. 2, 85748, Garching, Germany
[4] Warsaw University Observatory, Aleje Ujazdowskie 4, 00-478, Warsaw, Poland
[5] Universitá degli studi di Milano, via Celoria 31, 20131, Milano, Italy

Abstract. Removal of systematic effects is crucial in present and future CMB experiments mapping large fraction of the sky. Accurate CMB measurements ask for multi-feed array instruments observing the sky with a redundant scanning strategy covering the same sky region on different time scales and with different detectors for a better control of systematic effects. We investigate the capability to suppress $1/f$ noise features in Time Ordered Data (TOD) by using the destriping technique described in Maino et al. (1999), under realistic assumptions for crossing condition between different scan circles and sky signal fluctuations on small angular scales. We perform, as a working case, PLANCK-LFI simulated observations with few arcminutes pixel size convolved with LFI beam resolutions. In the noiseless case for crossing condition based on pixels with side larger than the input one, the destriping algorithm inserts extra-noise in the final map of the order of $\sim\mu$K in rms and few μK in peak-to-peak amplitude at 30 GHz. However including instrumental noise (white and $1/f$ noise) in the TOD, the impact of the sky signal on the destriping is found to be very small. In addition, for crossing condition based on pixels with side half of the one of the final map (typically $\sim1/3$ of the FWHM), we find only a small improvement ($\sim1\%$ level) in the destriping quality with respect to the case when crossings are searched on pixels with same size of the final map one. We can conclude that the receiver noise is the driver for destriping quality. We extend the analysis to high values of the knee frequency and find that, although significantly suppressed by destriping, the residual additional noise rms is $\sim31\%$ larger than the pure white noise rms at $f_{\rm k} = 1$ Hz which could be a critical issue in the extraction of CMB angular power spectrum. We verified that the approximation of the $1/f$ noise on averaged scan circles as a single baseline still works well even for these high values of the knee frequency. Furthermore, by comparing simulations with different noise levels and different sampling rates, we find that the destriping quality does not significantly depend on the receiver sensitivity whereas it improves proportionally to the improvement of sampling rate. Therefore given a noise level, the higher the sampling rate, the better the destriping quality. This paper is based upon PLANCK-LFI activities.

Key words. methods: data analysis – cosmology: cosmic microwave background

1. Introduction

In recent years a substantial improvement in measurements of Cosmic Microwave Background (CMB) radiation has taken place leading to several CMB anisotropy detections which support the gravitational instability scenario for structures formation (Smoot et al. 1992; Górski et al. 1996) and a universe with $\Omega_0 \sim 1$ (Miller et al. 1999; De Bernardis et al. 2000; Balbi et al. 2000; Pryke et al. 2001). A more complete analysis of current data implies multi-dimensional fits to jointly constrain several cos-

mological parameters (e.g. Lineweaver 1998; Tegmark & Zaldarriaga 2000). These estimations relay always on the accuracy by which foreground emissions and experimental systematic effects are known and properly accounted for. One of the major problems in present and future CMB anisotropy experiments, are all those possible systematic effects which affect the experiments in several ways.

In this respect a space mission is the optimum being free from the unwanted contamination from ground and Earth atmosphere emission. The Microwave Anisotropy Probe (MAP^1) satellite (Bennett 1996) by NASA has begun its mission aimed at all-sky imaging of the last

---

[1] http://map.gsfc.nasa.gov/

scattering surface of CMB photons, at several frequencies and with high angular resolution. In 2007 the PLANCK satellite[2] (Mandolesi et al. 1998; Puget et al. 1998) by ESA, will probe the very early phase of the Universe with even higher spectral coverage, sensitivity and angular resolution. Both satellites will operate around the L_2 Lagrangian point of the Sun-Earth system. This will allow a considerable rejection of the Sun, Earth and Moon radiation (see, e.g., Burigana et al. 2000), and the adopted redundant scanning strategy observing the same sky region several times on different time scales and by different detectors, allows a high control of systematic effects. In particular, PLANCK is a third generation of CMB mission, covering the widest frequency range ($\nu \sim$ 30–900 GHz) ever probed, necessary for a high accuracy subtraction of foreground contamination, and reaching a sensitivity per $0.3°$ pixel size of few μK at each frequency channel $\nu \lesssim 400$ GHz. Therefore an accurate monitoring and removal of systematic effects is crucial to reach the planned scientific objectives.

In the context of the PLANCK-LFI (Low Frequency Instrument) a detailed study of the major sources of systematic effects has been carried out. Burigana et al. (1998) and Mandolesi et al. (2000a) considered the impact of main beam distortions on CMB observations. Maino et al. (1999) took into account the problem of the so-called $1/f$ noise due to gain fluctuations in HEMT amplifiers in PLANCK-LFI receivers. A detailed study of the Galactic straylight contamination in LFI observations has been carried out by Burigana et al. (2001), where the effects of optical distortions are compared with the $1/f$ noise contamination.

The $1/f$ noise typically leads to stripes in the final map (Janssen et al. 1996) altering the statistical properties of the cosmic signal which is particularly relevant for CMB anisotropy. This effect can be parameterized by the knee-frequency f_k (i.e. the frequency at which the white and $1/f$ noise power spectra are equal) which should be as small as possible with respect to the spin-frequency of the satellite (e.g. for PLANCK $f_s = 0.0167$ Hz corresponding to 1 r.p.m. spin velocity). It is therefore crucial to properly correct this effect both by hardware and software techniques. The LFI, pseudo-correlation receivers, are properly designed to reduce the $1/f$ noise (Bersanelli et al. 1995). Delabrouille (1998) has implemented a technique for destriping PLANCK observations starting from the Time Ordered Data (hereafter TOD) and taking advantage of the redundancy of the PLANCK scanning strategy. Maino et al. (1999) have considered a similar technique in the more specific context of PLANCK-LFI observations and using the current theoretical predictions on LFI receiver properties. The results show that the destriping quality is remarkably good, except for the degenerate case in which all the crossings between different scan circles are concentrated very close to the ecliptic poles.

Although destriping algorithms are sometimes considered approximations of proper map making algorithms (recently implemented for large data time ordered data by, e.g., Natoli et al. 2001; Dore et al. 2001) they should be considered as methods to remove drifts in the TOD's and returning TODs cleaned from many classes of systematic effects (see, e.g., Mennella et al. 2001 for an analysis of periodic fluctuations). This is more suitable for many data analysis purposes directly on TODs such as monitoring of variable and transient sources (Terenzi et al. 2001). In the following analysis we make use of maps obtained by co-adding the TOD's cleaned by destriping codes: this way of proceed is one of the possible methods to quantify the quality of the destriping algorithms.

A key issue of destriping techniques is the operative definition of crossing between two different scan circles, since these techniques are based on the condition that the observed temperatures in the sky have to be the same for identical sky directions, although the samplings are taken along different scan circles at different times. Of course one can be more or less restrictive on the definition of the crossing condition: a more restrictive definition therefore may reduce the number of crossing possibly affecting the destriping quality while a less one may insert an extranoise due to the different sky signals in the two not exactly coincident sampling directions.

Another issue is the validity of the $1/f$ noise drift approximation in terms of a constant baseline (offset) for each averaged scan circles (or significant fraction of it), which in general holds as long as f_k is not far larger than f_s. Of course, the values of f_k appropriate to LFI receivers will be probed in future real hardware analysis. It is therefore interesting to assess the maximum values of f_k for which the destriping algorithm still works well removing $1/f$ noise stripes at a level which does not compromise the determination of CMB angular power spectrum.

In this paper we want to address these issues, evaluate the impact of different crossing conditions for different models of the microwave sky, including instrumental noise. Furthermore we push the knee-frequency to extremely high, and hopefully unrealistic, values ($\sim$1 Hz) to evaluate the destriping quality also for pessimistic cases.

We want to stress the fact that, although applied for the specific case of the PLANCK mission, these arguments are relevant to almost any CMB anisotropy observations. In typical CMB experiments, the scanning strategy implies repeated observations of the same sky regions on different time scales such as, e.g., BEAST (Seiffert 1996), COSMOSOMAS (Watson 1997). Note that the actual implementation of our destriping algorithm is completely independent of the details of the scanning strategy and of the pixelisation scheme[3].

---

[3] Our first implementation (Burigana et al. 1997b) worked in fact with the QUAD-CUBE scheme and the subsequent applications (Maino et al. 1999) with the HEALPix scheme (Górski et al. 1998) did not imply any modification at all.

This paper is organized as follows. We briefly describe the PLANCK scanning strategy and the generation of the TOD's in Sect. 2. The basic recipes of our destriping technique and the discussion of the crossing conditions are presented in Sect. 3. We report our simulation results in Sect. 4, where we assess the impact of the choice of crossing condition and intrinsic sky fluctuations on destriping quality. We dedicate Sect. 5 to the evaluation of the impact of possible high values of the knee-frequency on the destriping quality. We discuss there also the dependence of the destriping efficiency on the instrumental parameters (sensitivity and sampling rate) at different frequencies and introduce the functional form for noise power spectrum after destriping. Finally, we discuss our results and draw our conclusions in Sect. 6.

2. PLANCK observations

2.1. Scanning strategy

The orbit selected for PLANCK satellite will be a tight Lissajous orbit around the L_2 Lagrangian point of the Sun-Earth system (Mandolesi et al. 1998; Puget et al. 1998). The spacecraft spins at ~ 1 r.p.m. ($f_s \sim 0.0167$ Hz) and, in the simplest scanning strategy, the spin axis is essentially kept on the antisolar direction at constant solar aspect angle by a re-pointing of $2.5'$ every hour[4]. The LFI and HFI (High Frequency Instrument) share the focal plane of an Aplanatic telescope (see, e.g., Mandolesi et al. 2000b for a discussion on the advantages of this configuration) of 1.5 meter size which field of view is at an angle $\alpha = 85°$ from the spin-axis. Therefore PLANCK will trace large circles in the sky. In the nominal 14 mission months $\sim 10\,200$ spin-axis positions will be exploited covering twice nearly the whole sky, some regions of which will be covered three times. The actual sampling frequency (i.e. the frequency at which the sky signal is sampled along a given scan circle) adopted for LFI is about 3 samplings per FWHM resulting in a different number of samplings at the four LFI frequencies.

The details of the scanning strategy are not yet frozen and it may or not include a precession of the spacecraft spin axis about another axis kept along the antisolar direction re-pointed of $2.5'$ every hour.

2.2. From TOD to sky maps

We have implemented a code ("Flight Simulator", Burigana et al. 1997b, 1998; Maino et al. 1999) simulating the PLANCK scanning strategy and observations and applied to the study of some systematic effects. The relevant geometrical inputs of the code are the angle α between pointing and spin axis, beam position on the focal plane as well as beam response function. Other inputs are parameters describing the noise properties of the receivers.

We adopt here the nominal PLANCK scanning strategy, i.e. with 14 months of mission and re-pointing of the spin-axis every hour by $2.5'$ assuming 3 samplings per FWHM, and refer in this section to the case of simulations at 30 GHz where the nominal resolution (FWHM) is $33'$. The generation of instrumental noise is performed directly in Fourier space and FFT transformed back in real space (see Maino et al. 1999 for details).

We use the HEALPix pixelisation scheme (Górski et al. 1998), which is the adopted baseline for PLANCK products. The output of our Flight Simulator code are 4 matrices: $\mathbf{N}$, with pointing pixel number at specified resolution (usually larger than the beam size for a proper sampling of beam resolution), $\mathbf{T}$, with sky temperature plus full noise (white $+ 1/f$ noise), $\mathbf{W}$, with sky signal plus white noise only and $\mathbf{G}$, with sky signal only. Each matrix has n_s rows equal to the number of spin axis positions ($n_s \sim 10\,200$) and n_p columns equal to the number of samplings, weakly dependent on α, along a scan circle ($n_p \sim 1980$ at 30 GHz). The matrices $\mathbf{W}$ and $\mathbf{G}$ are computed to evaluate respectively the degradation of $1/f$ with respect ideal white noise case and the impact of the scanning strategy geometry on the observed signal.

From these TOD we build sky maps: making use of $\mathbf{N}$, possibly degraded at the desired resolution of the final map, and $\mathbf{T}$ we simply coadd the temperatures of those pixels which are observed several times during the mission. In the same way we build maps with only white noise, from $\mathbf{W}$, and, using $\mathbf{G}$, without receiver noise.

3. Definition of the problem

As first pointed out by Janssen et al. (1996) the effect of $1/f$ noise can be seen as one additive level (baseline or offset) different for each scan circle (or significant fraction of it). Since we work with scan circles averaged over 1-hour period, we strongly reduce drifts within the circle and we are left with the "mean" $1/f$ noise level for that observing period. Furthermore average is like a low-pass filter operation and, as long as the f_k is not far larger than f_s, this leaves only the very low frequencies components of the $1/f$ noise. Therefore it is a good approximation to model the effect of $1/f$ noise on the averaged scan circles as a single baseline A_i. We want to recover these baselines in order to properly adjust the signal.

3.1. Destriping technique

The destriping technique considered here, developed by Burigana et al. (1997b) and by Maino et al. (1999), has been derived from the COBRAS/SAMBA Phase A study proposal (Bersanelli et al. 1996) and from a re-analysis of Delabrouille (1998).

The first logical step of this method is the search of the crossings, i.e. to find the common pixels observed from different scan circles. This can be done at the desired resolution, not necessarily the same of the final map, if poorer than that at which the pixel stream is computed

---

[4] This simple scanning strategy provides also a smooth and quite uniform sky coverage which covers $\gtrsim 99\%$ of the full sky.

and stored. Let us indicate with N_{il}, T_{il} and E_{il} the pixel number, the observed signal and the "white" noise level for the pixel in the ith row (scan circle) and jth column (sampling along the circle) in matrices $\mathbf{N}$, $\mathbf{T}$ and $\mathbf{(W\text{-}G)}$ respectively. Let also be π the index that identifies a generic pair of observations of the same pixel: of course the index π is related to two elements in the matrix $\mathbf{N}$: $\pi \to (il, jm)$ where i and j are the indexes for two different scan circles and l and m the respective position of the observed pixel.

Following Maino et al. (1999) baselines are recovered solving the linear system:

$$\sum_{\pi=1}^{n_c} \left[\frac{[(A_i - A_j) - (T_{il} - T_{jm})] \cdot [\delta_{ik} - \delta_{jk}]}{E_{il}^2 - E_{jm}^2} \right]_\pi = 0 \qquad (1)$$

for all the $k = 1, ..., n_s$ (here δ is the usual Kronecker symbol). This simply translates into a set of n_s linear equation:

$$\sum_{h=1}^{n_s} C_{kh} A_h = B_k, \quad k = 1, ..., n_s \qquad (2)$$

which can be easily solved: the matrix of the coefficients C_{kh} is positive defined, symmetric and non singular. This last property is verified provided that there are enough intersections between different scan circles. A detailed discussion on the solving of system in Eq. (2) and RAM requirements can be found in Burigana et al. (1997b).

3.2. Crossing condition and sky map resolution

It is clear that the capabilities of the destriping technique to recover circles baselines strongly depend on the distribution of crossing points and on the quantity of crossings between different scan circles. Of course, these properties are correlated to each other and depend on the scan angle α, the beam position on the telescope field of view, the selected scanning strategy and, finally, on the definition of the crossing condition. This concept is parameterized in our code by the size of the pixel in which two samplings on two different scan circles have to fall to be considered as a "crossing". Maino et al. (1999) demonstrated that for $\alpha = 90°$ an off-axis beam (typical LFI position with $(\theta_B, \phi_B) = (2.8°, 45°)$ in the focal plane) destripes better than an on-axis beam ($\theta_B = 0°$ or $\phi_B = 0°$ or $\phi_B = 180°$) since for the former the crossing points are spread on a large region around the Ecliptic polar caps while, for the latter, they are practically only at the poles causing the system in Eq. (2) to be almost degenerate.

In order to better clarify the impact of the crossing condition on the destriping quality, let us consider the situation depicted in Fig. 1: here filled circles represent samples along two crossing scan circles while the cross indicates the crossing point. This could be regarded as a typical situation in which no sample could be associated to the crossing point.

Therefore one possibility would be to interpolate the signals (and consequently the noise) of the two samplings to the crossing points and feed the result into Eq. (2) as
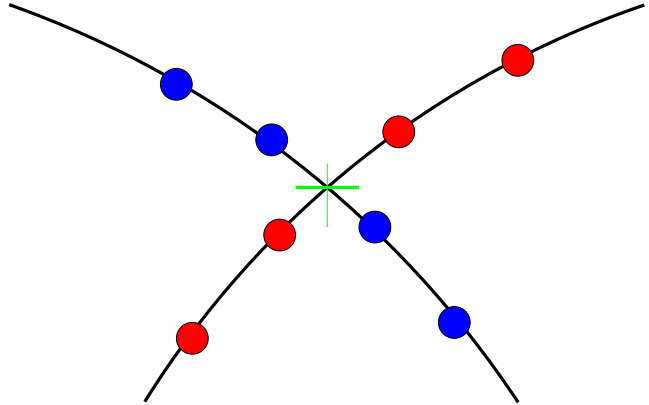
Fig. 1. Schematic representation of the crossing between two scan circles: filled circles are samplings along the circles.

in Revenu et al. (1999). We prefer not to interpolate but address the problem in a different way although our approach is formally equivalent to interpolation if only CMB is considered. However when considering foreground emission from point sources, that have large power on small angular scales, interpolation is no more practicable and may lead to large errors. We identify pointings by means of HEALPix pixel numbers at a suitable resolution and two pointings are considered coincident if they have the same pixel identification number. This however leaves an uncertainty: pointings can fall into the same pixel but could not be exactly coincident. This makes the signal of the two samplings different due to small scales fluctuations of sky signal due to CMB and foreground emissions.
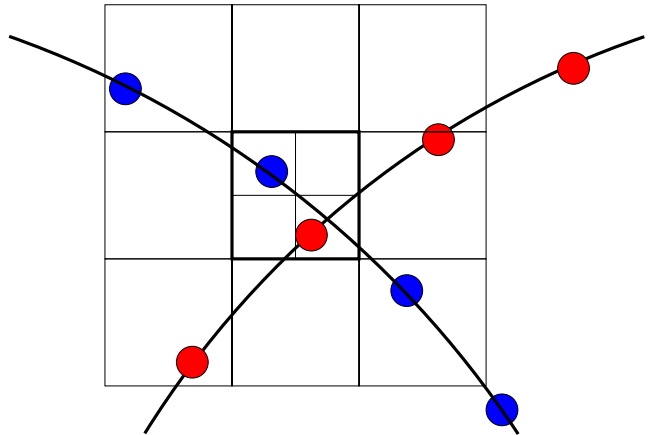
Fig. 2. Two samplings falling in the same crossing pixel (the thick one): the "true" pointings instead fall into different input map pixels with different sky signal that introduces an "extra" noise.

Since the sky signal has power also on small angular scales (e.g., due to discrete point sources) it is crucial to have a sky pixelised with the highest possible resolution in order to follow these fluctuations. It is also important to have a crossing pixel dimension small enough to be as close as possible to the real samplings along the scan circles. The ideal case would be having a map with super-resolution

and performing the crossing search at a resolution closer to the angular dimension of a single sampling. Only in this case is it possible to evaluate the true capabilities of a destriping algorithm. However it is not necessary to go to very high resolution ($\lesssim 1'$) since, at least for LFI, the highest resolution is $10'$ at 100 GHz, which means $\simeq 3.3'$ per samplings.

Reducing the crossing pixel size has the effect of dramatically lowering the number of crossings between scan circles, possibly affecting the destriping quality. It is however worth to note that the crossings are $\gtrsim 10^7$ (on a pixel $\gtrsim 3.5'$, see, e.g., Table 1) while baselines to be determined are at least 3 orders of magnitude less. In the next section we will present accurate simulations that quantify the impact on the destriping quality of sky signal fluctuations on small angular scales and crossing accuracy between scan circles.

4. Simulations

We consider input maps with $\mathcal{N}_{\mathrm{side}} = 1024$ corresponding to $3.5'$ pixel size. We use the baseline for the PLANCK scanning strategy with $\alpha = 85°$ and the spin-axis always on the Ecliptic plane. Beam position in the focal plane is chosen to be a worst case with respect the distribution of crossings between scan circles: crossings are limited to a small region around the polar caps. Within the actual focal plane arrangement this results in a position $(\theta_B, \phi_B) \sim (4°, 180°)$.

Our sky model is composed by primordial CMB anisotropy according to a standard CDM model[5] normalized to $COBE$, plus a model for the Galactic emission. This model has the spatial template of Galactic dust emission as in Schlegel et al. (1998) which has high angular resolution and therefore includes signal fluctuations on small scales. The emission of this map has been normalized to take into account dust, free-free and synchrotron emission at 30 GHz as derived from $COBE$-DMR data (Kogut et al. 1996). A realization of extra-galactic point sources has been derived from number source counts extracted from a Poissonian distribution (Toffolatti et al. 1998).

4.1. Pure sky signal

We want to evaluate the impact of intrinsic sky signal distribution on the destriping. To quantify the effect, we first consider simulations with no instrumental noise. The search for common pixels between different scan circles is based upon pixels with size $\geq 3.5'$. The output map has pixel size of $13.7'$ which is close to the Nyquist frequency for the 30 GHz beam FWHM. After destriping we subtract the "destriped" map from the map obtained simply co-adding pixels according to the scanning strategy. As we expect we found a small excess of noise since pixels that are considered coincident by the destriping algorithm,

have indeed different sky signals (e.g. see Fig. 2). The destriping algorithm tries to adjust this signal difference as if it was due to different offsets in the scan circles. In Fig. 3 we show the residual extra noise (hereafter REN) for the sky model which includes extra-galactic point sources: stripes are clearly inserted by the destriping code.

In Table 1 we report rms and peak-to-peak amplitude of the REN as a function of the dimension of pixel used for searching for common observations between scan circles. The input signal includes a pure CMB sky, CMB plus Galactic signal and CMB plus Galactic emission and extra-galactic radio sources. The results at 30 GHz are clearly the worst case for LFI with respect to the contribution of foreground emissions.

Of course, when the crossing pixel has the same size of pixel input map, the effect is zero as expected and therefore we do not report this results. The REN increases, as expected when enlarging the crossing pixel size, particularly for the case with extra-galactic point sources due to their power on very small angular scales. The situation with pure CMB sky is less dramatic due to the smooth sky gradient.

Note that the rms and peak-to-peak amplitude of the effect lie in the range $0.4-1.4\,\mu$K and $\sim 6.0-8.6\,\mu$K respectively on a pixel of $13.7'$. These numbers have to be compared with the expected sensitivity at 30 GHz re-scaled to $13.7'$ pixel size, which is of the order of 15 μK. It is important to remind that the goal for the *overall* budget for systematic effects is few μK and this effect could contribute in principle in non negligible way to the budget.

### 4.2. Sky signal and full noise

We include in our simulations the effect of instrumental white and $1/f$ noise with a knee frequency of about 0.1 Hz. The sky signal include CMB, Galactic emission and extra-galactic radio sources (this is close to a realistic scenario).

To assess the impact of sky signal fluctuations and crossing condition on the destriping efficiency we compare two sets of simulations: the first with pure noise and the second with noise plus signal. In both cases, as in Sect. 4.1, the output map has $13.7'$ pixels while searching for crossing is performed at $13.7'$ and $6.8'$. Any difference between the two cases indicates the impact of sky signal and crossing condition on destriping quality.

Results show that pure noise case is almost identical to the case which includes sky signal: differences in REN are of the order of 0.13% and 0.56% when crossings are searched on $6.8'$ and $13.7'$ pixels sizes respectively. Furthermore we find very little improvement in destriping quality when crossings are based on pixel sizes smaller that the one of the final map (typical differences are below 0.5%).

This means that the quantity which determines the destriping quality is the noise component while the sky signal plays a minor role adding only small degradation.

---

[5] $\Omega_{\mathrm{CDM}} = 0.95, \Omega_{\mathrm{b}} = 0.05$ and $H_0 = 50$ km/s/Mpc.

−4.38e−003 ■■■■ 4.38e−003
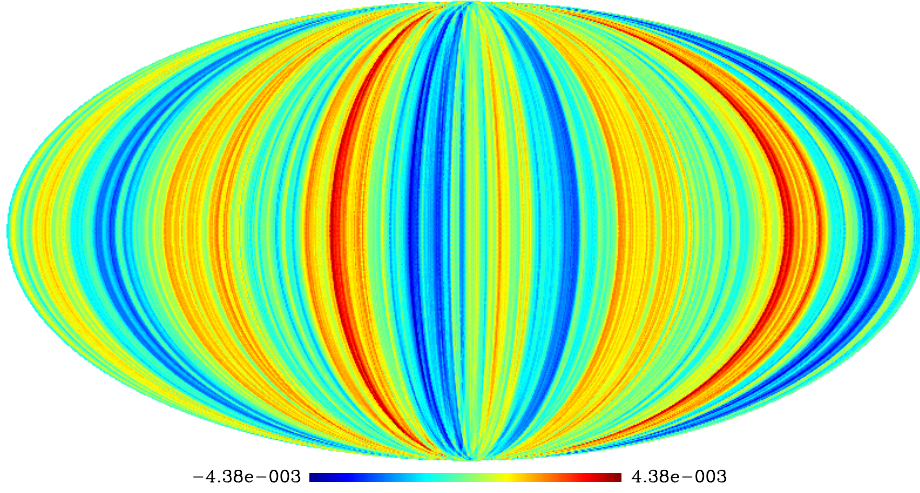
Fig. 3. Residual stripes after subtraction of the "destriped" map with pure sky signal and the input map for a model including extra-galactic sources and using a crossing pixel dimension of 13.7′. Units are mK at 30 GHz. Note that the effect in principle could be relevant being around 8 μK in peak-to-peak amplitude.

Table 1. Peak-to-peak amplitude and rms of the REN as a function of the crossing pixel size for CMB,CMB + Galaxy and CMB + Galaxy + Extra-galactic sources.

Xing pixel	# pairs	rms	peak-to-peak
CMB			
6.8′	$\sim 2 \times 10^7$	0.386 μK	2.57 μK
13.7′	$\sim 7 \times 10^8$	0.959 μK	5.97 μK
CMB + Galaxy			
6.8′	$\sim 2 \times 10^7$	0.387 μK	2.58 μK
13.7′	$\sim 7 \times 10^8$	0.960 μK	5.97 μK
CMB + Galaxy + Extra-galactic Sources			
6.8′	$\sim 2 \times 10^7$	0.615 μK	4.16 μK
13.7′	$\sim 7 \times 10^8$	1.408 μK	8.62 μK
CMB + Galaxy + Extra-galactic Sources + Noise			
6.8′	$\sim 2 \times 10^7$	31.884 μK	286.37 μK
13.7′	$\sim 7 \times 10^8$	31.881 μK	288.39 μK
Pure noise			
6.8′	$\sim 2 \times 10^7$	31.889 μK	286.11 μK
13.7′	$\sim 7 \times 10^8$	31.871 μK	285.78 μK

A crucial estimator of the $1/f$ stripes impact on CMB anisotropy measurements is its angular power spectrum. It can be directly compared to the CMB angular power spectrum and with the spectra that characterize other classes of both instrumental and astrophysical contaminations.

In the case of instrumental pure white noise and in the limit of full sky coverage the angular power spectrum is given by

$$C_\ell \simeq \frac{4\pi}{N_{\text{pix}}^2} \sum_{i=1}^{N_{\text{pix}}} \sigma_i^2, \tag{3}$$
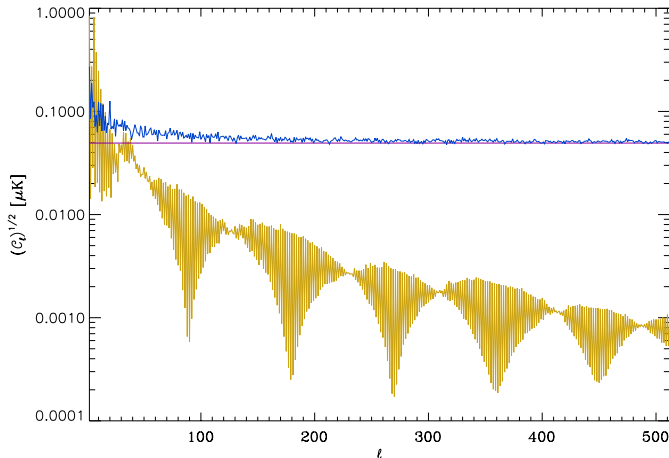
Fig. 4. Angular power spectrum of the REN for the pure signal case (CMB + Galaxy + Extra-galactic sources; grey line), compared with the level of the white noise power spectrum (straight solid line) and the noise spectrum after destriping (pure noise case – solid line).

where σ_i is the noise in the ith pixel and N_{pix} is the total number of pixels.

In Fig. 4 the angular power spectrum of the REN for the pure signal case (CMB + Galaxy + Extra-galactic sources) is shown compared with the expected level of white noise and the noise spectrum after destriping (pure noise case). It is clear that most of the excess at low ℓs is due to residual $1/f$ noise after destriping (see Maino et al. 1999). For higher ℓ ($\gtrsim$50), where the destriping algorithm works better and the noise spectrum is almost white, the contamination is below the white noise level. This again underlines the small impact of signal correlation in the destriping algorithm and, furthermore, leads to the conclusion that, in this realistic case of sky signal and instrumental noise, the destriping algorithm does not introduce extra-correlation since the residual after subtraction of the input sky is almost white noise plus a residual $1/f$.

5. Destriping quality versus knee-frequency

Since the sky signal contributes only marginally to the destriping quality when instrumental noise is included, we concentrate our attention on instrumental noise only with increasing values of the knee-frequency. We proceed with the analysis of high values of the knee-frequency, up to 1 Hz. This in principle might impact the destriping quality because the filter applied to the data (i.e. the mean over 1-hour period) could not be adequate and so the constant baseline approximation of residual noise

5.1. Simulations at 30 GHz

We explore the intervals of f_k ranging from 0.025 Hz up to 1 Hz: the former being derived from theoretical computation as in Burigana et al. (1997a) and Seiffert et al. (2001), the latter being a pessimistic conservative case. These knee-frequencies span from values comparable with

Table 2. Amplitude of the fractional REN before and after destriping and the corresponding ratio as a function of the knee-frequency.

f_k [Hz]	Before [%]	After [%]	Ratio
0.025	63.6	1.13	56.3
0.1	177.8	3.71	47.9
0.4	427.9	13.4	31.9
1.0	725.7	30.7	23.6

the spin frequency to values ~100 times larger. Note that for LFI the baseline requirement is set to $f_k < 0.05$ Hz. The output map has the usual 13.7′ resolution and the crossing pixel size is 13.7′ following the results of previous section.

In Table 2 we report results of the fractional, compared to the white noise, REN rms before and after destriping, together with their ratio. It is clear the increasing degradation for increasing f_k after destriping: this reaches value of 13% to 30% of the white noise rms at 0.4 and 1 Hz respectively. The ratio is another indicator of destriping degradation: it decreases and will approach unity for extreme high values of f_k. It is however interesting to note the small range of values exploited by the ratio compared to the wide range in f_k indicating a good capability of destriping to control the residual noise.

The increase of the degradation for increasing knee-frequency would have an impact on the angular power spectrum obtained inverting the sky map after destriping. In Fig. 5 we report the angular power spectra before and after destriping for $f_k = 0.1$ Hz (left) and $f_k = 1$ Hz (right) respectively. The height of the blobs increases as well as the low-multipole tail of the residual noise. This of course could be a problem in the extraction of the CMB angular power spectrum in particular if the structures related to low-ℓ tail show a non-Gaussian distribution. This can be verified by Wiener filtering residual noise map taking the low-ℓ tail as a signal and subtract from it the white noise level derived from the high multipoles. It can be shown that only for very low f_k the distribution of the residual noise could be approximated as a Gaussian, while for larger f_k stripes appear: this is indeed the level of stripes that the destriping algorithm is not able to remove since it is completely embedded into white noise. However this effect has to carefully considered in CMB data analysis in presence of $1/f$ noise.

We also consider simulations at 30 GHz with $f_k = 0.4$ and 1 Hz in which we try to recover two baselines per circle instead of a single baseline. After destriping the level of extra noise is around ~14% and ~31%, respectively for $f_k = 0.4$ and 1 Hz almost the same as in the single baseline case. This means that despite the fact the $f_k \simeq 60 \times f_s$, a single baseline is a good approximation of the averaged $1/f$ noise.
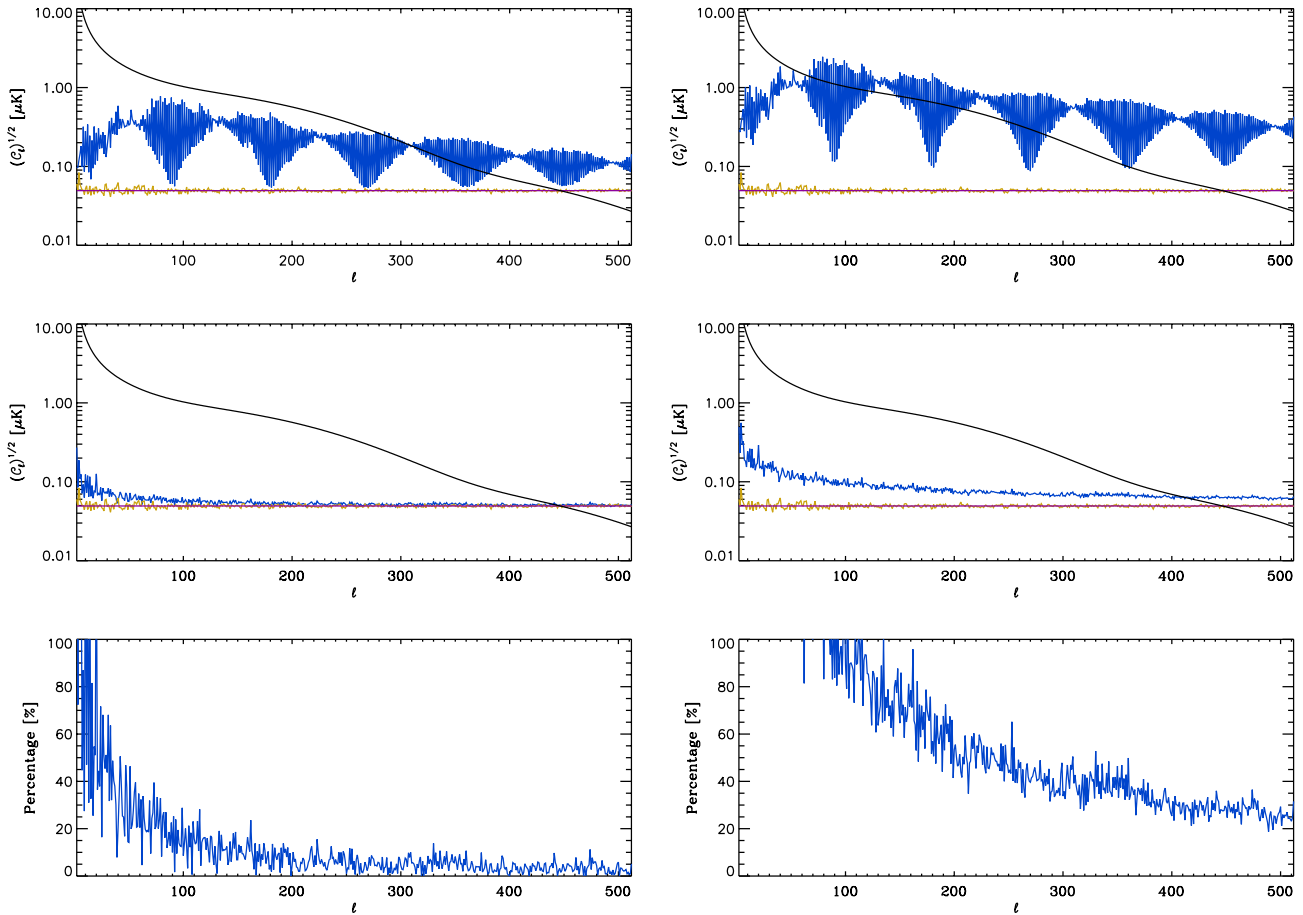
Fig. 5. Angular power spectrum before (top) and after (middle) destriping for $f_{\rm k} = 0.1$ Hz (left) and for $f_{\rm k} = 1$ Hz (right) compared to the theoretical level of the white noise and the CMB power spectrum convolved with the nominal FWHM at 30 GHz. In the bottom panel the residual noise in percentage of white noise level is reported as a function of multipole.

5.2. Dependence on the sampling per circle: simulations at 100 GHz

To complete our estimates on the dependence of the destriping efficiency and of the residual $1/f$ noise on the instrumental parameters at different frequencies we extended our simulations to include a case with a larger number of samplings per scan circle.

We performed simulations, including only instrumental noise, at LFI 100 GHz channel that has a nominal angular resolution of $10'$ and a noise level per unit integration time which is about 3–4 times larger than a single channel at 30 GHz. We exploit the same geometrical configuration of the previous 30 GHz case and $f_{\rm k} = 0.4$ Hz. Output maps are at $\mathcal{N}_{\rm side} = 1024$ with $3.5'$ pixel size that is appropriate for the $10'$ angular resolution. Crossings between scan circles are searched for on $3.5'$ and $1.75'$ pixel size. For both cases we obtain the same results: the fractional REN after destriping is $\sim 4.3\%$ of the white noise.

For further checking the dependence of destriping quality upon white noise level and number of samples along a scan circle, we carried out another simulation with the same parameters as before but with the white noise level properly scaled in order to have the same noise level per

unit integration time as at 30 GHz. We obtain a fractional REN after destriping of $\sim 4.4\%$ of the white noise level, almost equal to the previous result. Comparison with results in Sect. 5.1 indicates that, for the same value of the knee-frequency and white noise level, the larger the number of samplings along a scan circle, the better destriping quality is achieved.

5.3. Upper limits on the $1/f$ noise impact

As shown above, the residual $1/f$ noise contamination after the destriping, expressed in terms of fractional additional noise with respect the pure white noise, significantly decreases with increasing sampling rate.

In our simulations we have located the beams in a worst-case position regarding the destriping quality assuming an angle $\alpha = 85°$ and a scanning strategy without precession of the spin-axis. The inclusion of the precession although affecting the distribution of integration time per pixel, might partially increase the destriping performance (Maino et al. 1999).

In addition Burigana et al. (2001) have shown that the quality of the destriping algorithm is not significantly affected by the main beam distortion effect and by the beam

rotation. The interpretation of this result is analogous to that discussed in Sect. 4 to explain the results of Table 1: differences of few μK between the two signals (without noise) of a crossing used in the destriping algorithm, due either to the underlying different sky or to different beam orientations, are overwhelmed by the instrumental noise fluctuations.

These considerations strongly indicate that the results reported in Table 2, strictly holding for the configuration considered there, can be regarded as more general upper limits applying to the residual $1/f$ noise contamination after destriping. We can then exploit the results of Table 2 to derive analytical upper limits for the extra noise after destriping with respect to the case of pure white noise as a function of the knee-frequency. Fitting the results we obtain a power law of the form:

$$\log(\text{rms}) \lesssim 0.898 \times \log(f_{\text{k}}) - 0.517 , \qquad (4)$$

where rms is expressed in terms of white noise level (%) and f_{k} is in Hz. The accuracy in rms of Eq. (4) is $\lesssim 4\%$ in the explored range of f_{k}.

6. Discussion and conclusions

We have reported here a detailed study on removal of $1/f$ noise features in CMB observations directly on TODs to obtain cleaned TODs. For this purpose we have made use of the destriping algorithm developed by Burigana et al. (1997b) and Maino et al. (1999) taking into account the impact of intrinsic sky signal fluctuations on the angular scale used to recover common observations between different scan circles and by extending the range of the most relevant instrumental parameters, such as sensitivity, knee frequency and sampling rate.

We have verified that, with pure sky signal in absence of noise, relaxing the crossing condition has the effect of introducing REN which appears as stripes in the map. This is particularly important when including the contribution coming from radio sources in simulated input sky. The typical rms effect is of the order of 0.6 μK and shows peak-to-peak amplitude of 7 μK at 30 GHz. This effect, although small, may be in principle important since the overall budget for systematic effects for LFI is of few μK. On the other hand, we find that this effect is practically eliminated when the instrumental noise is taken into account, since the noise component is the dominant one.

We explore a wide range of possible values of knee-frequency from 0.01 Hz up to 1 Hz. The extra noise after destriping increases with increasing values of f_{k} and we derive an analytical expression for the upper limits of the residual $1/f$ noise contamination in terms of fractional excess of noise with respect to the pure white noise case. In the worst case the residual contamination may be relevant if the knee frequency is not strongly reduced via hardware; for example, for $f_{\text{k}} = 0.4$ Hz (1 Hz) we find a fractional REN of about 13% (30%).

We have verified that a single baseline approximation in the use of the destriping code is still valid even for high values of the knee frequency, since up to $f_{\text{k}} = 1$ Hz no significant improvement is found by using two baselines per scan circle.

Furthermore we find that the destriping quality is only very slightly improved when crossings are searched on pixels smaller than the ones of the final map.

Finally, our simulations at 100 GHz show that the destriping quality does not depend on the intrinsic white noise level, whereas it improves about proportionally to the number of samplings along the scan circle. Analogously, from the comparison with the results obtained in a previous simulation work (Maino et al. 1999), we find that the current PLANCK 2.5$'$ shift in spin axis re-pointing, better than the 5$'$ shift of the Phase A study, provides a better sampling along the azimuthal direction which further improves the destriping quality.

This extensive study of the destriping algorithm capabilities and dependencies upon different configurations confirms the robustness of the technique and allows to improve its use. Furthermore the general approach of this technique, allow its application to most of the present and future CMB experiments where a redundant scanning strategy is considered. In CMB observations the complexity and the mixing of many classes of instrumental and astrophysical systematic effects requires a particular care. In fact new detailed analyses based on both measured hardware performances provided by laboratories tests and on a more detailed description of instrument and mission parameters (including focal plane assembly, scanning strategy, detailed knowledge of sampling strategies) will be carried out in the future.

References

Balbi, A., Ade, P., Bock, J., et al. 2000, ApJ, 545, L1
Bennett, C. L. 1996, Amer. Astron. Soc. Meet., 88.05
Bersanelli, M., Mandolesi, N., Weinreb, S., Ambrosini, R., & Smoot, G. F. 1995, Int. Rep. TeSRE/CNR, 177/1995
Bersanelli, M. Y., Bouchet, F. R., Efstathiou, G. et al. 1996, ESA, COBRAS/SAMBA Report on the Phase A study, D/SCI(96)3
Burigana, C., Seiffert, M., Mandolesi, N., & Bersanelli, M. 1997a, Int. Rep TeSRE/CNR, 186/1997, March
Burigana, C., Malaspina, M., Mandolesi, N., et al. 1997b, Int. Rep TeSRE/CNR, 198/1997, November [astro-ph/9906369]
Burigana, C., Maino, D., Mandolesi, N., et al. 1998, A&AS, 130, 551
Burigana, C., Natoli, P., Vittorio, N., Mandolesi, N., & Bersanelli, M. 2000, Int. Rep. TeSRE/CNR, 272/2000, April

Burigana, C., Maino, D., Górski, K. M., et al. 2001, A&A, 373, 345

De Bernardis, P., Ade, P. A. R., Bock, J. J., et al. 2000, Nature, 404, 955

Delabrouille, J. 1998, A&AS, 127, 555

Górski, K. M., Banday, A. J., Bennett, C. L., et al. 1996, ApJ, 464, L11

Górski, K. M., Hivon, E., & Wandelt, B. D. 1998, Proc. of the MPA/ESO Conf. on Evolution of Large-Scale Structure: from Recombination to Garching, ed. A. J. Banday, R. K. Sheth, & L. Da Costa, 37, [astro-ph/9812350]

Janssen, M., Scott, D., White, M., et al. 1996, [astro-ph/9602009]

Kogut, A., Hinshaw, G., Banday, A. J., et al. 1996, ApJ, 464, L5

Lineweaver, C. H. 1998, ApJ, 505, L69

Maino, D., Burigana, C., Maltoni, M., et al. 1999, A&AS, 140, 383

Mandolesi, N., et al. 1998, Planck LFI, A Proposal Submitted to the ESA

Mandolesi, N., Bersanelli, M., Burigana, C., et al. 2000a, A&AS, 145, 323

Mandolesi, N., Bersanelli, M., Burigana, C., & Villa, F. 2000b, Astroph. Lett. Comm., 37, 151

Mennella, A., Bersanelli, M., Burigana, C., et al. 2001, A&A, submitted, [astro-ph/0111078]

Miller, A. D., Caldwell, R., Devlin, M. J., et al. 1991, ApJ, 524, L1

Pryke, C., Halverson, N. W., Leitch, E. M., et al. 2001, submitted to ApJ, [astro-ph/0104490]

Puget, J. L., et al. 1998, HFI for the Planck Mission, A Proposal Submitted to the ESA

Revenu, D., Kim, A., Ansari, R., et al. 1999, A&AS, 142, 499

Schlegel, D. J., Finkbeiner, D. P., & Davis, M. 1998, ApJ, 500, 525

Seiffert, M. 1996, Amer. Astron. Soc. Meet., 189, #88.03

Seiffert, M., Mennella, A., Burigana, C., et al. 2001, Rev. Scient. Intrum., to be submitted

Smoot, G. F., Bennett, C. L., Kogut, A., et al. 1992, ApJ, 396, L1

Tegmark, M., & Zaldarriaga, M. 2000, ApJ, submitted, [astro-ph/0002091]

Terenzi, L., Bersanelli, M., Burigana, C., et al. 2001, Proc. of the 2K1BC Workshop, Experimental Cosmology at millimetre wavelengths, 9–13 July 2001, Breuil-Cervinia (AO), AIP Conf. Proc., in press

Toffolatti, L., Argüeso Gómez, F., De Zotti, G., et al. 1998, MNRAS, 297, 117

Watson, R. 1997, Proc. of the Spanisch Relativity Meet., ed. J. Buitrago, E. Madiavilla, & A. Oscoz, 103